Discrete multi-physics simulations of diffusive and convective mass transfer in boundary layers containing motile cilia in lungs

Ariane, Mostapha; Kassinos, Stavros; Velaga, Sitaram; Alexiadis, Alessio

DOI:
10.1016/j.compbiomed.2018.01.010

Document Version
Peer reviewed version

Citation for published version (Harvard):
Ariane, M, Kassinos, S, Velaga, S & Alexiadis, A 2018, 'Discrete multi-physics simulations of diffusive and convective mass transfer in boundary layers containing motile cilia in lungs', *Computers in Biology and Medicine*, vol. 95, pp. 34-42. https://doi.org/10.1016/j.compbiomed.2018.01.010

Discrete multi-physics simulations of diffusive and convective mass transfer in boundary layers containing motile cilia in lungs

Mostapha Ariane[a], Stavros Kassinos[b], Sitaram Velaga[c], Alessio Alexiadis[a]

[a] School of Chemical Engineering, University of Birmingham, Edgbaston Birmingham B15 2TT, United Kingdom

[b] Department of Mechanical and Manufacturing Engineering, University of Cyprus, 1678 Nicosia, Cyprus

[c] Pharmaceutical Research Group, Division of Medical Science, Department of Health Science, Luleå University of Technology, 971 87 Luleå, Sweden

Abstract

In this paper, the mass transfer coefficient (permeability) of boundary layers containing motile cilia is investigated by means of discrete multi-physics. The idea is to understand the main mechanisms of mass transport occurring in a ciliated-layer; one specific application being inhaled drugs in the respiratory epithelium. The effect of drug diffusivity, cilia beat frequency and cilia flexibility is studied. Our results show the existence of three mass transfer regimes. A low frequency regime, which we called shielding regime, where the presence of the cilia hinders mass transport; an intermediate frequency regime, which we have called diffusive regime, where diffusion is the controlling mechanism; and a high frequency regime, which we have called convective regime, where the degree of bending of the cilia seems to be the most important factor controlling mass transfer in the ciliated-layer. Since the flexibility of the cilia

and the frequency of the beat changes with age and health conditions, the knowledge of these three regimes allows prediction of how mass transfer varies with these factors.

Keywords: Discrete Multi-Physics, Smoothed Particle Hydrodynamics, Mass-Spring Model, cilia, diffusivity, mass transfer

1. Introduction

Motile cilia are hair-like structures present on the surface of a variety of cells. They are found in large numbers in the human body and beat in coordinated waves to perform a number of different functions. For instance, in the conducting and central airways of the lungs, cilia are surrounded by mucus that traps particulate materials and pathogens. The coordinated motion of the cilia propels these materials towards the pharynx where they are swallowed or expelled via coughing, a phenomenon known as mucociliary clearance or mucociliary escalator [1]. Mathematical modelling of this phenomenon has attracted the interest of various researchers in material, biological and pharmaceutical sciences. The main motivation is to understand the factors controlling the effectiveness of mucociliary clearance since this is important in the context of environmental exposure (see [2] for a detailed review). [3] introduced an analytical model of a mucus layer with cilia motion. Their findings suggested that the mucus flow in contact with the airway is governed by a viscosity gradient in the mucus layer, but in this work, the cilia were only considered as rigid rods. Later, [4] implemented a more realistic cilia motion model including effective and recovery stroke in a two layers system. The outcomes highlighted the role of the cilia penetration (in the mucus layer) on the mucus transport effectiveness. At the beginning of the new century, [5] focused their researches on the mucus draining in an idealised rigid bronchial tree with an air flow effect. Their model showed the viscosity-dependence of the mucus transport as well as the important role of the

geometry. The emergence of the Immersed Boundary Method (IBM) has allowed a significant enhancement in mucociliary clearance modelling. [6] studied the effects of the velocity, the viscosity, the beat cilia frequency, the number of cilia and the depth of the periciliary layer. The main results showed that (i) the velocity of the periciliary fluid is linearly proportional to the cilia beat frequency, (ii) the mucus viscosity plays a little role on the mucus flow rate contrary to the number of cilium which increases the mucus transport, and (iii) a minimum depth of periciliary layer is needed to generate a mucociliary transport. [7] extended the two-dimensional [6] model to a three-dimensional representation and thus were able to capture the cilia motion in the normal direction; they confirmed the previous results. Additionally, the same authors in another publication [8], focused on cilia dysfunction and malformation. They emphasized the negative effects of too elastic and too rigid cilia beat patterns on the mucus transport. Then, a method coupling IBM with a lattice Boltzmann method was used by [9] to implement an Oldroyd-B model and to simulate a viscoelastic fluid. They found that an increase of the mucus viscosity accelerates the movement of mucus layer. [10] with a penalty technique, also concentrated their researches on genetic cilia diseases and defective mucus clearance using a non-Newtonian model. They correlated, in the case of cystic fibrosis, mucus velocity and rheology with a mucus maturation model and highlighted that shear-thinning mucus can accentuate agglomeration phenomena in regions with ineffective clearance. Most of the previous studies have focused on the altered effectiveness of mucociliary clearance under disease states, for example in primary or acquired ciliary dyskinesia. Here, we also take a look how impairments to the ciliary function can modify the speed with which pollutants, irritants and toxic agents can reach the airway epithelium.

While mucociliary escalator is one of the major defence mechanisms protecting the lungs, it has important implications in pulmonary drug delivery. In the case of inhaled aerosolized

medicines, mucociliary clearance competes with the particle dissolution and absorption that eventually determines the lung bioavailability of the inhaled drugs [11]. Smaller particles trapped in the mucus layer progressively dissolve and diffuse towards the epithelium and the drug gets absorbed (Fig. 1a). On the other hand, larger or slowly dissolving particles are partly cleared by the ciliary action, thus reducing the amount of drug absorbed (Fig. 1b). Mucociliary clearance concerns the mass transfer of particles trapped in the mucus layer to the pharynx for clearance, whilst the drug absorption depends on the diffusion of particles towards the epithelium through the mucus and the ciliated-layer. The role that the cilia beat pattern plays as part of the mucociliary clearance mechanism has been studied in the past. While the cilia beat is also likely to affect mass transfer, to the best of our knowledge, it has received no attention in the literature from this perspective.

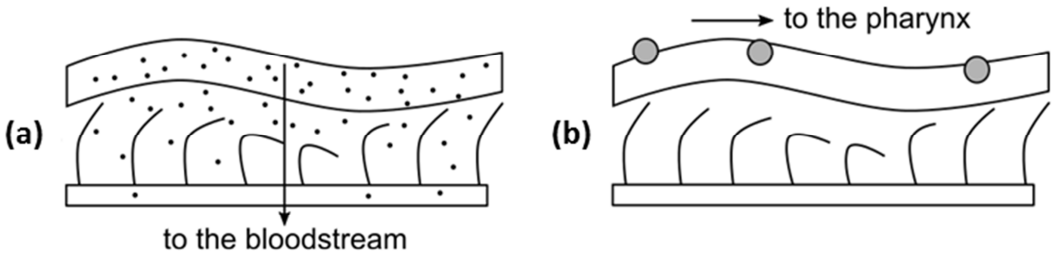

Fig. 1. Drug absorption (a) versus mucociliary clearance (b).

In this work, we use a modelling technique called discrete multi-physics [12-17] to investigate how the motion of the cilia affects mass transfer conditions in the ciliated-layer. By means of discrete multi-physics, the following research questions are addressed. Does the presence of the cilia enhance or hinder the mass transfer in the ciliated layer? For example, it is known that smoking, age, and health conditions affect the frequency of the cilia beat [18]. Thus, it is of interest to understand how drug absorption is sensitive to the frequency of the beat. Finally,

88 does the flexibility of the cilia, which also depends on age and health conditions [19], play a
89 role too?

90 Answering these questions can provide insights not only to the development of inhalation
91 medicines, or to the dynamics of harmful chemicals during environmental exposure, , but also
92 the design of artificial cilia needed for lab-on-a-chip or organ-on-a-chip applications [20].

93 **2. Preliminary considerations and background**

94 *2.1 Cilia beat*

95 In the past, several studies [21-27] have investigated the cilia motion in the respiratory
96 epithelium. The results are not always fully consistent with each other (e.g. Fig. 2), but in
97 general, the cilia motion is divided into two phases: an 'effective stroke', in which the cilia
98 move forward and propel the mucus layer in the same direction; and a 'recovery stroke', in
99 which the cilia return to their initial position.

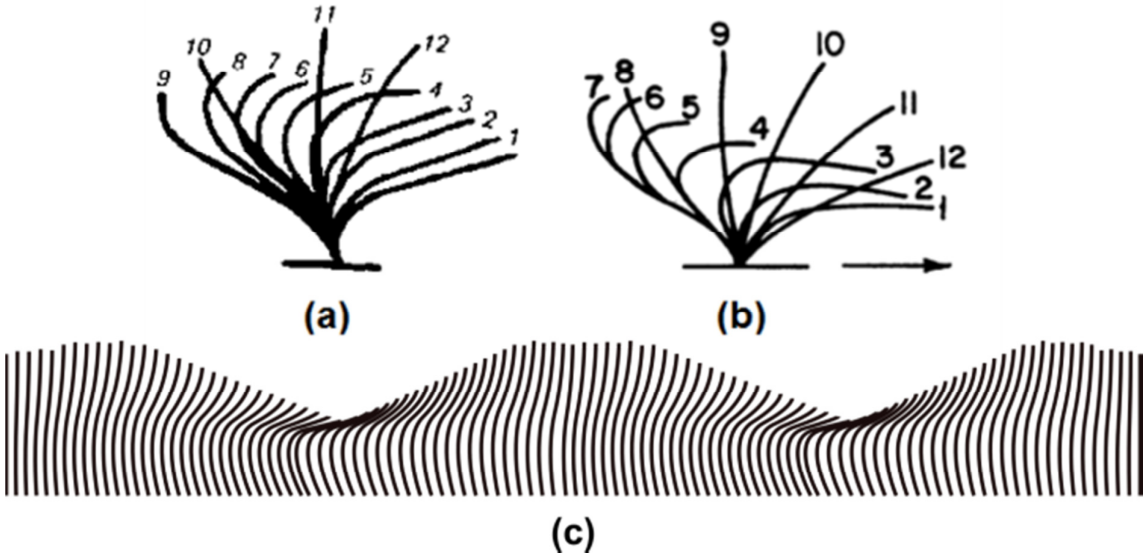

100

Fig. 2. Cilium's motion according to (a) Sanderson and Sleigh [22] and (b) Aiello and Sleigh [21] and (c) metachronal wave.

Moreover, the movement of each cilium (Fig. 2) is coordinated with that of the others producing a wave-like overall motion known as metachronal wave. A variety of cilia beat frequencies in the range between 3 and 20 Hz have been observed in the respiratory epithelium, with the frequency being a function of temperature, age and health conditions [25-27]. Artificial cilia used in lab-on-a-chip applications, on the other hand, can reach higher frequencies in the order of 50 Hz [28].

2.2 Membrane permeability and mass transfer

In general, the rate of absorption of a certain drug into the body depends on the permeability P_{me} [m s^{-1}] of the cellular membrane to that specific drug. In experiments, the drug's flux through the membrane J [kg m^{-2} s^{-1}] is measured and the permeability calculated from

$$J = P_{me}(c_1 - c_2), \tag{1}$$

where $c_2 - c_1$ [kg m^{-3}] is the difference of drug's concentration across the membrane (Fig. 3a).

If before permeating the membrane, the drug diffuses through an additional mass transfer resistance (e.g. the layer of mucus), the total permeability P_{TOT} of the mucus + the membrane layer is given by

$$\frac{1}{P_{TOT}} = \frac{1}{P_{me}} + \frac{1}{P_{mu}}, \tag{2}$$

where P_{mu} is the drug's permeability of the mucus layer.

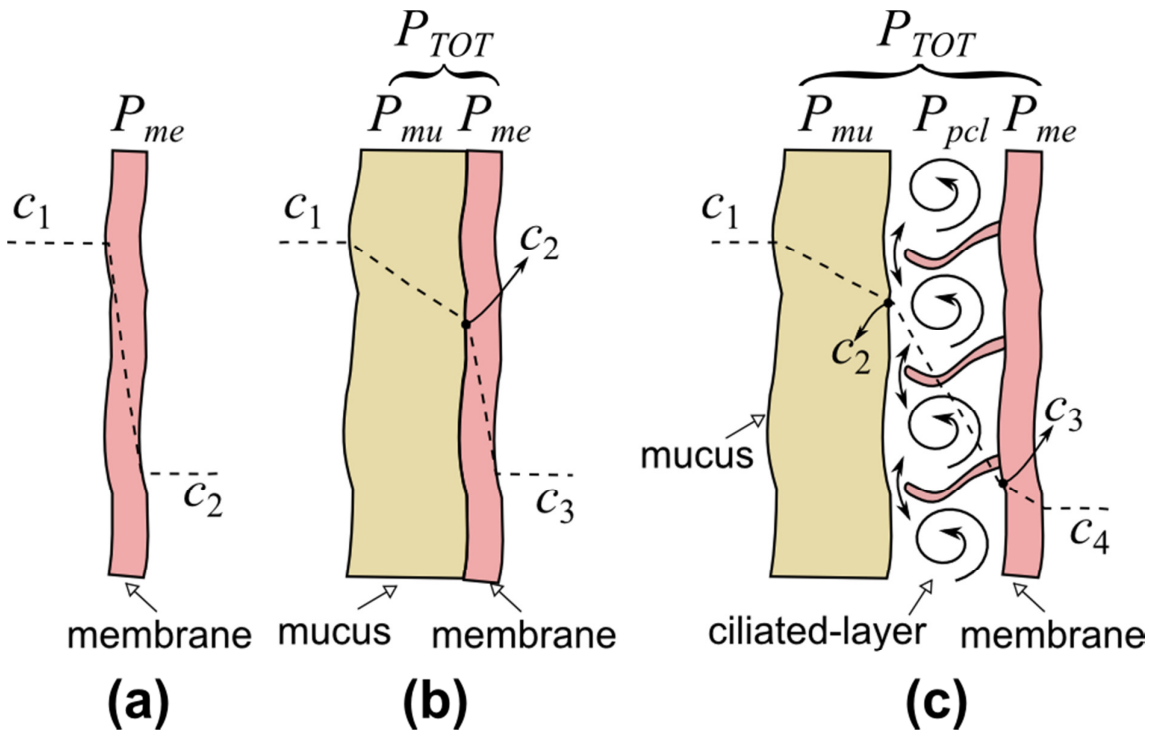

Fig. 3. Permeability through a membrane (epithelium), (b) permeability through membrane + mucus, (c) permeability through membrane + mucus + ciliated-layer.

In the respiratory epithelium, between the mucus layer and the membrane, there is a third layer, the periciliary layer (PCL), where a low-viscosity fluid is agitated by motile cilia. The overall permeability of the mucus + ciliated + membrane layer is, therefore,

$$\frac{1}{P_{TOT}} = \frac{1}{P_{me}} + \frac{1}{P_{mu}} + \frac{1}{P_{pcl}}, \tag{3}$$

where P_{pcl} is the permeability of the ciliated−layer.

126 Permeability is the term mostly used in biology and medicine; in physics and engineering, it is
127 often replaced by the molecular diffusivity D [m^2 s^{-1}], which is linked to permeability by the
128 relation

$$P = \frac{D}{\delta}, \tag{4}$$

129 where δ [m] is the thickness of the layer where the drug diffuses. There is, however, a
130 fundamental difference between mass transfer in the membrane or in the mucus layer, and in
131 the PCL. The diffusivities D_{me} (membrane) and D_{mu} (mucus) originate from
132 hydrodynamically static layers and only depend on the molecular interaction between the
133 diffusing drug and the diffusive medium; they can be measured from standard experiments,
134 which do not depend on hydrodynamics. The PCL, on the other hand, is hydrodynamically
135 active since the motion of the cilia generates recirculation regions where mass transfer
136 depends on convection rather than diffusion. Under certain conditions, discussed in Section
137 3.2, however, the dynamics can be considered pseudo-diffusive and an apparent diffusivity
138 coefficient D_{pcl} can be used to model the mass transport in the ciliated-layer. This means that
139 Eq. (3) can be rewritten as

$$\frac{\delta_{TOT}}{D_{TOT}} = \frac{\delta_{me}}{D_{me}} + \frac{\delta_{mu}}{D_{mu}} + \frac{\delta_{pcl}}{D_{pcl}}, \tag{5}$$

140 While D_{me} and D_{mu} are real diffusivities, which are constant for a given drug, D_{pcl} is a
141 pseudo-diffusivity, which also depends on the motion of the cilia. The goal of this paper is to
142 determine how the pseudo-diffusivity D_{pcl} is affected by the three parameters: (i) the
143 molecular diffusivity D of the drug in the periciliary fluid, (ii) the frequency f [s^{-1}] of the cilia

beat, and (iii) the flexibility of the cilia measured as bending length s [m] covered by the cilia during bending.

2.3 Soluble versus insoluble particles

Inhalation devices deliver medicines to the airways in the form of fine solid particles (typically in the range of 2 to 6 μm) or liquid droplets (aerosols). Particles that dissolve in the mucus gradually diffuse and reach the epithelium (Section 2.2). As discussed earlier, the fate of insoluble particles depends on their size. Particles larger than 6 μm are trapped in the mucus layer and eliminated by mucociliary clearance. Particles smaller than 6 μm, instead, can penetrate the mucus layer and diffuse similarly to molecules of soluble drugs. Their diffusivity D_B is the result of Brownian motion and can be calculated according to the Stokes-Einstein relation

$$D_B = \frac{k_B T}{3\pi\mu a}, \tag{6}$$

where k_B is the Boltzmann constant [kg m^2 s^{-2} K^{-1}], T [K] the temperature, μ [Pa s] the viscosity of the fluid and a [m] the diameter of the particle. Based on Eq. (6), in our analysis, we can treat soluble particles and small insoluble particles in the same way. The only difference being that the latter case requires the Brownian diffusivity D_B instead of the molecular diffusivity D.

3. Modelling Approach

To determine how the pseudo-diffusivity D_{pcl} depends on the molecular diffusivity, the beat frequency and the flexibility of the cilia, we use a computational approach called Discrete Multi-Physics (DMP) that links various discrete (i.e. particle based) modelling techniques in order to reach results not attainable with each technique separately. This method has been successfully tested for both solid-liquid flows [12-14] and fluid-structure interaction [15-17]. In this study, Smoothed Particle Hydrodynamics (SPH) is used to simulate the fluid, and the Mass-Spring Model (MSM) to simulate the membrane. A brief introduction to SPH and MSM is given in Appendix A and more details can be found in the aforementioned publications.

3.1 Geometry

Many modelling works on mucociliary clearance follows a 2D representation of the ciliated-layer (see [2] for a review); in this study, we also follow this approach. The computational domain (Fig. 4a) is divided into four regions: the mucus, the PCL, the cilia and the membrane. SPH particles are used to model the mucus and the PCL, MSM particles are used to model the cilia, while static SPH particles are used for the membrane. In the following, we refer to the particles used for the cilia as cilia-particles, to the particles used to model the mucus layer as mucus-particles, and so on. The computational box is shown in Fig. 4b. There are 36 cilia with length L_{pcl} = 5 μm each, the distance between cilia is l = 0.5 μm and the total length of the section investigated is W = 20 μm; since periodic boundary conditions in the x-direction are considered, each particle whose position is $x < 0$ or $x > W$ is reintroduced on the other side of the computational box. The actual computational domain, therefore, is defined as an infinite replica in the x-direction of the computational box illustrated in Fig. 4b. The thickness of the mucus layer in the simulation is H_{mu} 2 μm, which is lower than the actual mucus layer (typically 3-5 μm [29]). In this study, this is not a limitation since we are mostly interested in

185 the mass transport in the PCL and the mucus layer is only needed to determine the
186 concentration at the boundary conditions. A smaller mucus layer requires less computational
187 particles and allows faster simulations.

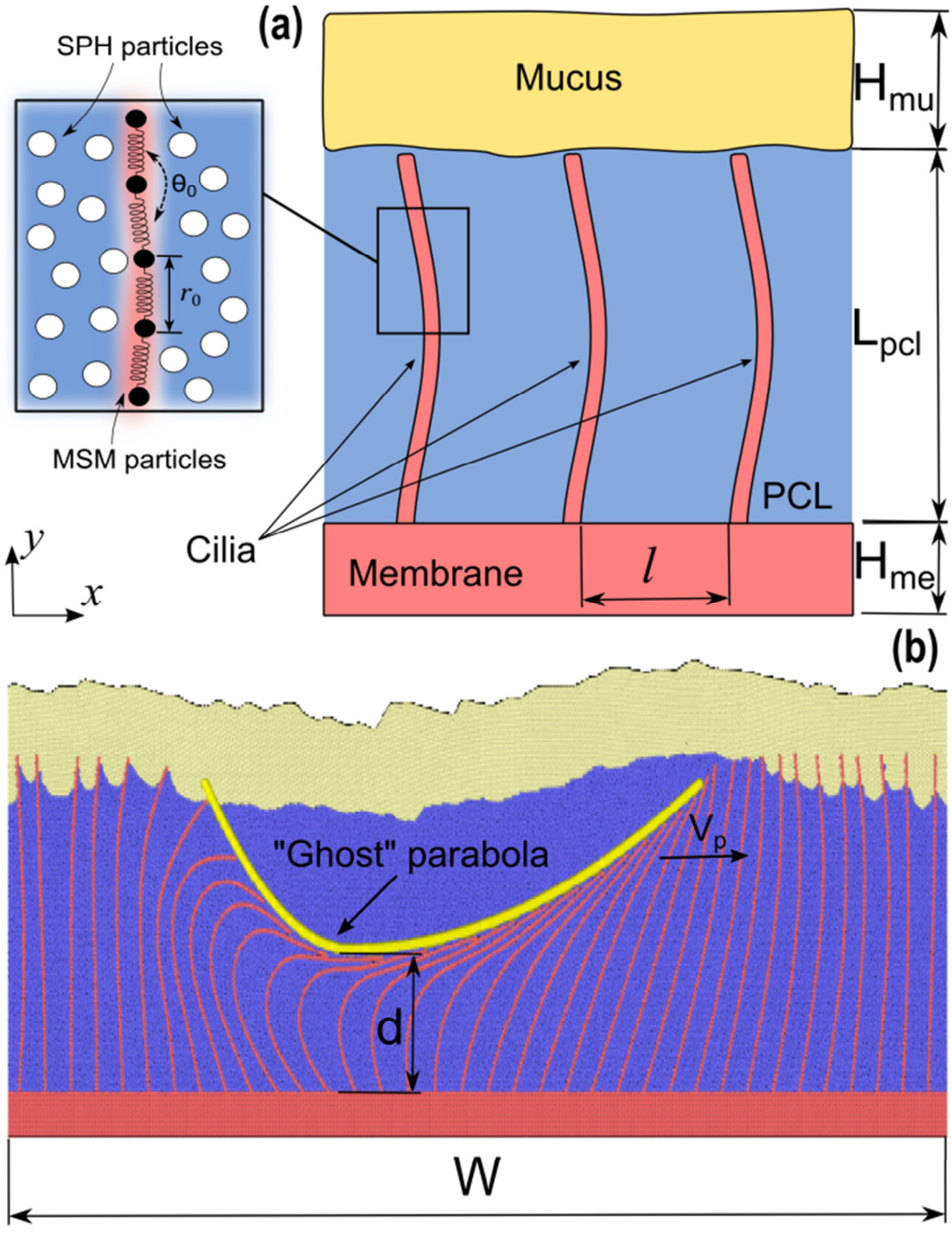

188

189 Fig. 4. The geometry of the PCL (a) and the computational box used in the simulations (b).

Modelling the *metachronal wave* of the cilia turned out to be a challenging task. If only a few cilia are considered, a series of time-dependent forces can be imposed to the cilia-particles resulting in an approximately correct bending and straitening motion of each cilium. When the number of cilia is above four or five, however, the interaction with the fluid produces a gradual loss of coordination among the cilia that, as time progresses, breaks the metachronal rhythm. We have tried a number of different strategies (based on forces applied to the cilia computational particles) to overcome this problem; the best solution we found consists of using a fifth type of 'ghost' particles that only interact, by means of a repulsive force (see Appendix A), with the cilia. These particles are arranged in a parabolic shape that moves horizontally (see Fig. 4b). The PCL fluid and the mucus do not feel the presence of these 'ghost' particles (no interaction forces), but if the parabola comes into contact with a cilium, the cilium bends and follows the outline of the parabola (interaction forces). When the parabola moves away, the cilium gradually recovers its original shape. In this way, the coordination of the *metachronal wave* is maintained for the entire duration of the simulation and the shapes obtained are consistent with those observed in the literature (Fig. 2). Given the periodic boundary conditions explained above, when the parabola exits the domain from $x = W$, it is re-introduced at $x = 0$. The velocity of the parabola v_P and the length of the domain W determine the frequency of the beat (i.e. $f = v_P/W$). The 'ghost' parabola is also used to investigate the effect of the flexibility of the cilia. During their motion, the cilia periodically bend and straighten and the degree of bending is an indication of how flexible the cilia are. By varying the distance d between the minimum of the parabola and the epithelium (Fig. 4b) we can vary the bending length and simulate cilia with different flexibilities. In the rest of the article, we refer at the distance $s = L_{pcl} - d$ as the bending length.

3.2 Dimensionless analysis

Our aim is to determine how the pseudo-diffusivity D_{pcl} depends on D, f and s. Dimensionless analysis indicates that the system can be described by only two dimensionless groups. The Sherwood number is defined as

$$Sh = \frac{D_{pcl}}{D}, \tag{7}$$

which expresses the ration between the molecular and the apparent diffusivity; and the Péclet number that, here, works as a dimensionless frequency

$$Pe = \frac{s^2 f}{D}. \tag{8}$$

In our results, therefore, we seek correlations of the type

$$Sh = KPe^n, \tag{9}$$

where K and n are two constants to be determined from the simulation data.

In the following sections, we will also use the geometric ratio

$$\lambda = \frac{s}{L_{pcl}}, \tag{10}$$

which is not a fundamental dimensionless group, but it will be used, during the discussion, to highlight some specific aspects that depend on the cilia flexibility.

226 **4. Results and discussion**

227 There are two types of parameters required for the simulations: model parameters and
228 simulation parameters. Model parameters define the SPH, MSM and DMP structures and are
229 fixed in all the simulations (Appendix B). Simulation parameters such as D, f and s, represent
230 the operative conditions and are varied as indicated in Table 1.

231

232 Table 1. List of simulations with diffusivities, frequencies and bending lengths parameters.

Case	D [m^2 s^{-1}]	f [Hz]	s [µm]	λ [-]	Pe [-]	D_{PCL} [m^2 s^{-1}]	Sh [-]
D10v05H3	$1\ 10^{-10}$	2.5	1.3	0.27	0.04	$3.08\ 10^{-11}$	0.31
D10v05H4	$1\ 10^{-10}$	2.5	1.9	0.38	0.09	$3.00\ 10^{-11}$	0.30
D10v05H5	$1\ 10^{-10}$	2.5	2.5	0.50	0.16	$3.04\ 10^{-11}$	0.30
D10v05H6	$1\ 10^{-10}$	2.5	3.1	0.62	0.24	$3.14\ 10^{-11}$	0.31
D10v1H3	$1\ 10^{-10}$	5.0	1.3	0.27	0.09	$3.06\ 10^{-11}$	0.31
D10v1H4	$1\ 10^{-10}$	5.0	1.9	0.38	0.18	$2.98\ 10^{-11}$	0.30
D10v1H5	$1\ 10^{-10}$	5.0	2.5	0.50	0.32	$3.01\ 10^{-11}$	0.30
D10v1H6	$1\ 10^{-10}$	5.0	3.1	0.62	0.47	$3.14\ 10^{-11}$	0.31
D10v2H3	$1\ 10^{-10}$	10.0	1.3	0.27	0.18	$3.05\ 10^{-11}$	0.30
D10v2H4	$1\ 10^{-10}$	10.0	1.9	0.38	0.36	$2.97\ 10^{-11}$	0.30
D10v2H5	$1\ 10^{-10}$	10.0	2.5	0.50	0.63	$3.03\ 10^{-11}$	0.30
D10v2H6	$1\ 10^{-10}$	10.0	3.1	0.62	0.95	$3.21\ 10^{-11}$	0.32
D11v05H3	$1\ 10^{-11}$	2.5	1.3	0.27	0.45	$3.59\ 10^{-12}$	0.36
D11v05H4	$1\ 10^{-11}$	2.5	1.9	0.38	0.90	$3.81\ 10^{-12}$	0.38
D11v05H5	$1\ 10^{-11}$	2.5	2.5	0.50	1.58	$4.21\ 10^{-12}$	0.42
D11v05H6	$1\ 10^{-11}$	2.5	3.1	0.62	2.37	$4.46\ 10^{-12}$	0.45
D11v1H3	$1\ 10^{-11}$	5.0	1.3	0.27	0.89	$3.57\ 10^{-12}$	0.36
D11v1H4	$1\ 10^{-11}$	5.0	1.9	0.38	1.79	$3.88\ 10^{-12}$	0.39
D11v1H5	$1\ 10^{-11}$	5.0	2.5	0.50	3.16	$4.41\ 10^{-12}$	0.44
D11v1H6	$1\ 10^{-11}$	5.0	3.1	0.62	4.75	$4.92\ 10^{-12}$	0.49
D11v2H3	$1\ 10^{-11}$	10.0	1.3	0.27	1.79	$3.77\ 10^{-12}$	0.38
D11v2H4	$1\ 10^{-11}$	10.0	1.9	0.38	3.59	$4.00\ 10^{-12}$	0.40
D11v2H5	$1\ 10^{-11}$	10.0	2.5	0.50	6.32	$4.52\ 10^{-12}$	0.45
D11v2H6	$1\ 10^{-11}$	10.0	3.1	0.62	9.50	$5.21\ 10^{-12}$	0.52
D12v2H3	$1\ 10^{-12}$	10.0	1.3	0.27	17.88	$5.31\ 10^{-13}$	0.53
D12v2H4	$1\ 10^{-12}$	10.0	1.9	0.38	35.87	$5.75\ 10^{-13}$	0.58
D12v2H5	$1\ 10^{-12}$	10.0	2.5	0.50	63.15	$6.94\ 10^{-13}$	0.69
D12v2H6	$1\ 10^{-12}$	10.0	3.1	0.62	94.99	$8.58\ 10^{-13}$	0.86
D11v10H3	$1\ 10^{-11}$	50.0	1.3	0.27	8.94	$3.90\ 10^{-12}$	0.39
D11v10H4	$1\ 10^{-11}$	50.0	1.9	0.38	17.94	$4.41\ 10^{-12}$	0.44
D11v10H5	$1\ 10^{-11}$	50.0	2.5	0.50	31.58	$5.27\ 10^{-12}$	0.53
D11v10H6	$1\ 10^{-11}$	50.0	3.1	0.62	47.49	$6.33\ 10^{-12}$	0.63
D10v0H3	$1\ 10^{-10}$	0.0	1.3	0.27	0.00	$3.12\ 10^{-11}$	0.31
D10v0H4	$1\ 10^{-10}$	0.0	1.9	0.38	0.00	$3.06\ 10^{-11}$	0.31
D10v0H5	$1\ 10^{-10}$	0.0	2.5	0.50	0.00	$3.06\ 10^{-11}$	0.31
D10v0H6	$1\ 10^{-10}$	0.0	3.1	0.62	0.00	$3.17\ 10^{-11}$	0.32
D11v0H3	$1\ 10^{-11}$	0.0	1.3	0.27	0.00	$3.61\ 10^{-12}$	0.36
D11v0H4	$1\ 10^{-11}$	0.0	1.9	0.38	0.00	$3.71\ 10^{-12}$	0.37
D11v0H5	$1\ 10^{-11}$	0.0	2.5	0.50	0.00	$3.86\ 10^{-12}$	0.39
D11v0H6	$1\ 10^{-11}$	0.0	3.1	0.62	0.00	$3.99\ 10^{-12}$	0.40
D12v0H3	$1\ 10^{-12}$	0.0	1.3	0.27	0.00	$6.38\ 10^{-13}$	0.64
D12v0H4	$1\ 10^{-12}$	0.0	1.9	0.38	0.00	$6.53\ 10^{-13}$	0.65
D12v0H5	$1\ 10^{-12}$	0.0	2.5	0.50	0.00	$6.48\ 10^{-13}$	0.65
D12v0H6	$1\ 10^{-12}$	0.0	3.1	0.62	0.00	$6.32\ 10^{-13}$	0.63
D12v10H3	$1\ 10^{-12}$	50.0	1.3	0.27	89.38	$7.65\ 10^{-13}$	0.76
D12v10H4	$1\ 10^{-12}$	50.0	1.9	0.38	179.36	$9.10\ 10^{-13}$	0.91
D12v10H5	$1\ 10^{-12}$	50.0	2.5	0.50	315.76	$1.17\ 10^{-12}$	1.17
D12v10H6	$1\ 10^{-12}$	50.0	3.1	0.62	474.94	$1.67\ 10^{-12}$	1.67
D10v10H3	$1\ 10^{-10}$	50.0	1.3	0.27	0.89	$3.36\ 10^{-11}$	0.34
D10v10H4	$1\ 10^{-10}$	50.0	1.9	0.38	1.79	$3.61\ 10^{-11}$	0.36
D10v10H5	$1\ 10^{-10}$	50.0	2.5	0.50	3.16	$3.97\ 10^{-11}$	0.40
D10v10H6	$1\ 10^{-10}$	50.0	3.1	0.62	4.75	$4.22\ 10^{-11}$	0.42
D10v5H3	$1\ 10^{-10}$	25.0	1.3	0.27	0.45	$3.05\ 10^{-11}$	0.30
D10v5H4	$1\ 10^{-10}$	25.0	1.9	0.38	0.90	$3.10\ 10^{-11}$	0.31
D10v5H5	$1\ 10^{-10}$	25.0	2.5	0.50	1.58	$3.36\ 10^{-11}$	0.34
D10v5H6	$1\ 10^{-10}$	25.0	3.1	0.62	2.37	$3.61\ 10^{-11}$	0.36

4.1 Metachronal wave and velocity profiles

The focus of this article is on mass transfer, but, since convection, which depends on the local velocity pattern, is an important means of mass transfer, in this section, we discuss the typical velocity profiles obtained from the simulations. Fig. 5a shows the shape of the *metachronal wave* obtained in the simulations by using the 'ghost parabola' approach. Concerning the velocity profile (Fig. 5b), the most important feature for convective mass transport is the large recirculation region occurring where the cilia bend. Higher velocities appear in other regions, but these are confined within adjacent cilia and, as explained in Section 4.2, they do not significantly increase mixing in the ciliated-layer. The penetration of the cilia in the mucus layer is approximately 0.5 μm, which is consistent with values in the literature [22]. The velocity of the mucus layer in our calculations is around 10 μm s^{-1}, which is consistent with the values reported in the literature (typically ranging from 10 − 60 μm s^{-1} [30].

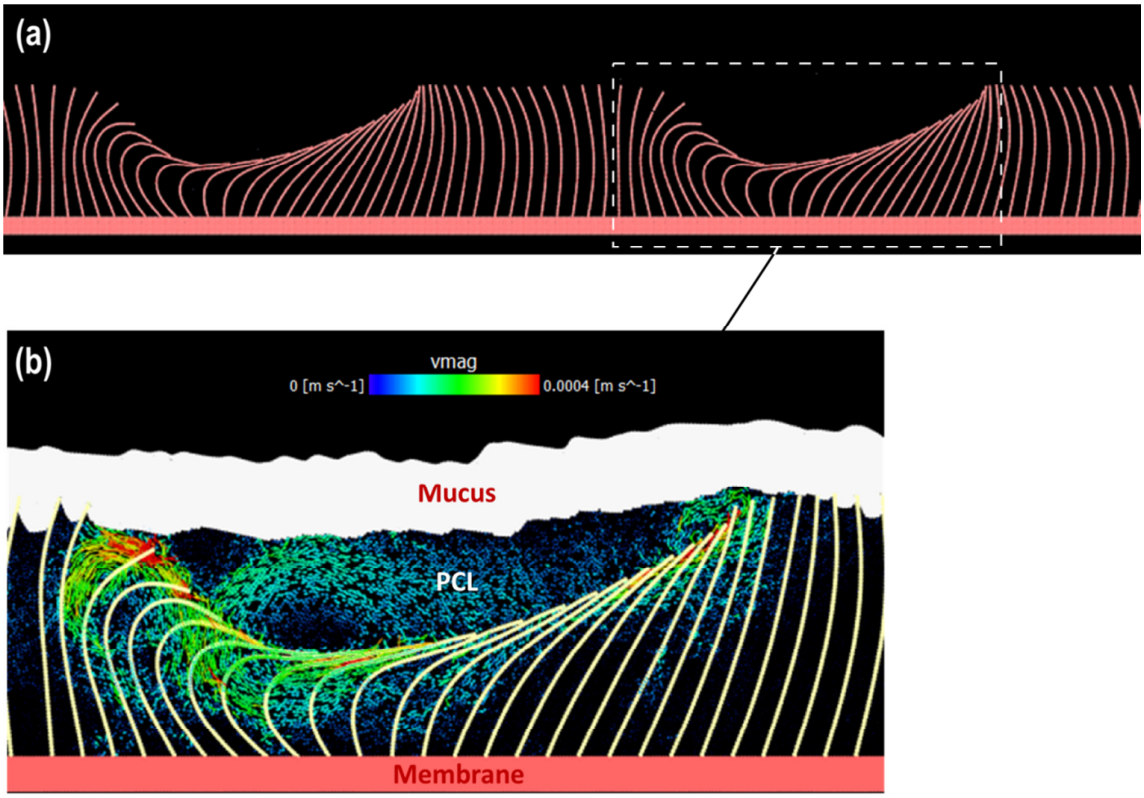

Fig. 5. *Metachronal wave* (a) and velocity profiles (b) for $D = 10^{-11}$ m^2 s^{-1}, $f = 10$ Hz, $s = 2.5$ µm.

4.2 Concentration profiles

In order to study the mass transfer within the PCL, we include in our model the equation of mass conservation of a chemical species A. How this is introduced in the discrete multi-physics model is explained in Appendix D (additional details are given in [13]). A typical concentration profile is shown in Fig. 6.

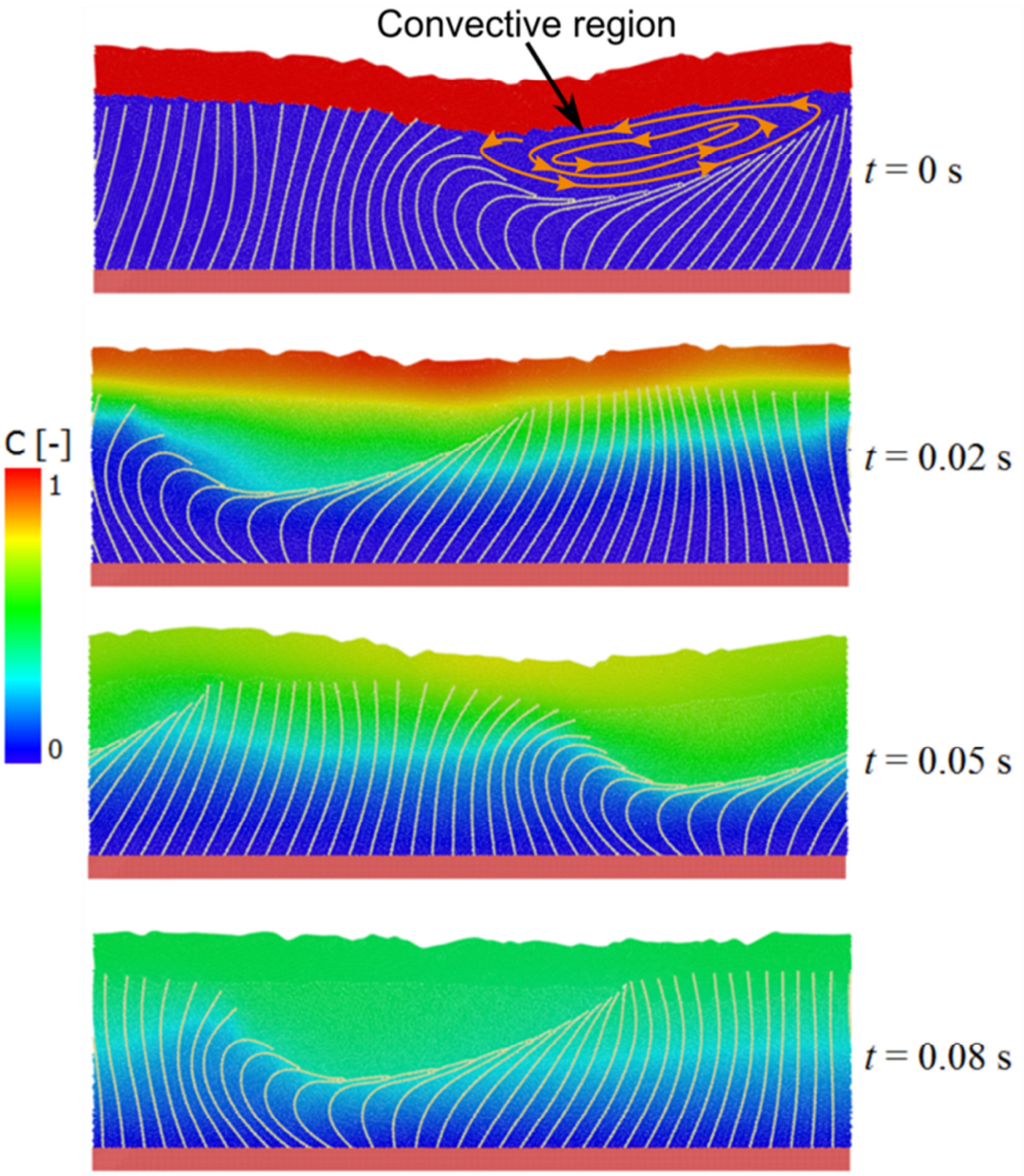

Fig. 6. Concentration profiles of the chemical species A at different time steps ($D = 10^{-11}$ m^2 s^{-1}, $f = 10$ Hz, $s = 2.5$ μm).

As the *metachronal wave* moves in the PCL, the bending of the cilia generates an empty region (free of cilia), called 'convective region' in Fig. 6, with characteristic size s, below the

mucus layer. This region has a large recirculation pattern that increases convective mass transport. Fig. 6 shows the effect of convection on a typical concentration profile. Initially, we assume all the drug is fully dissolved in the mucus layer and diffused in the PCL layer from there. The initial (dimensionless) drug concentration, therefore, is zero in the PCL and 1 in the mucus layer. The diffusivity of the drug is arbitrarily considered 10 times faster in the mucus than in the PCL, while the membrane is considered a passive wall with no mass exchange with the PCL. These boundary conditions allow for an effective calculation of D_{pcl} as explained in the next section.

4.3 Calculation of D_{pcl}

In order to calculate D_{pcl}, we need the instantaneous concentration profiles in the y-direction, which are calculated by averaging the concentration over the x-coordinate (Fig. 7a). Mass transfer in the PCL depends on a combination of diffusion and convection, however, under certain conditions the dynamics can be considered pseudo-diffusive and an apparent diffusivity coefficient D_{pcl} can be used to model mass transport in the ciliated-layer. We also assume that diffusivity of the drug is substantially larger in the PCL than in the membrane and we stop our simulation before the drug reaches the membrane. The usefulness of these assumptions can be understood from Eq. (3) and Fig. 3. From our simulations, we can only measure the total permeability P_{TOT} of the system. However, we want to calculate the permeability of the ciliated layer P_{pcl}. If we arbitrarily set the permeability in the mucus high, $1/P_{mu}$ in Eq. (3) can be neglected and, if we stop the simulation before the drug reaches the membrane, $1/P_{me}$ can neglect. Under these circumstances, therefore, $P_{TOT} \sim P_{pcl}$ and, by measuring P_{TOT} we estimate P_{pcl}. This is a sort of numerical 'trick', it has nothing to do with the real drug diffusion in the mucus, but allows to correctly estimate P_{pcl}. Once P_{pcl} is known,

realistic values of P_{TOT} can be calculated from Eq. (3) by introducing the actual values of P_{me} and P_{mu}.

Under the assumptions discussed above, the time-dependent concentration profiles in the PCL follow the formula [31]

$$c = c_{max} e^{-\frac{y^2}{4D_{pcl}t}}, \tag{11}$$

where c_{max} is the (time-dependent) concentration at $y = 0$, which depends on the total mass of drug dissolved in the mucus at the beginning of the simulation and decays with time as $t^{0.5}$.

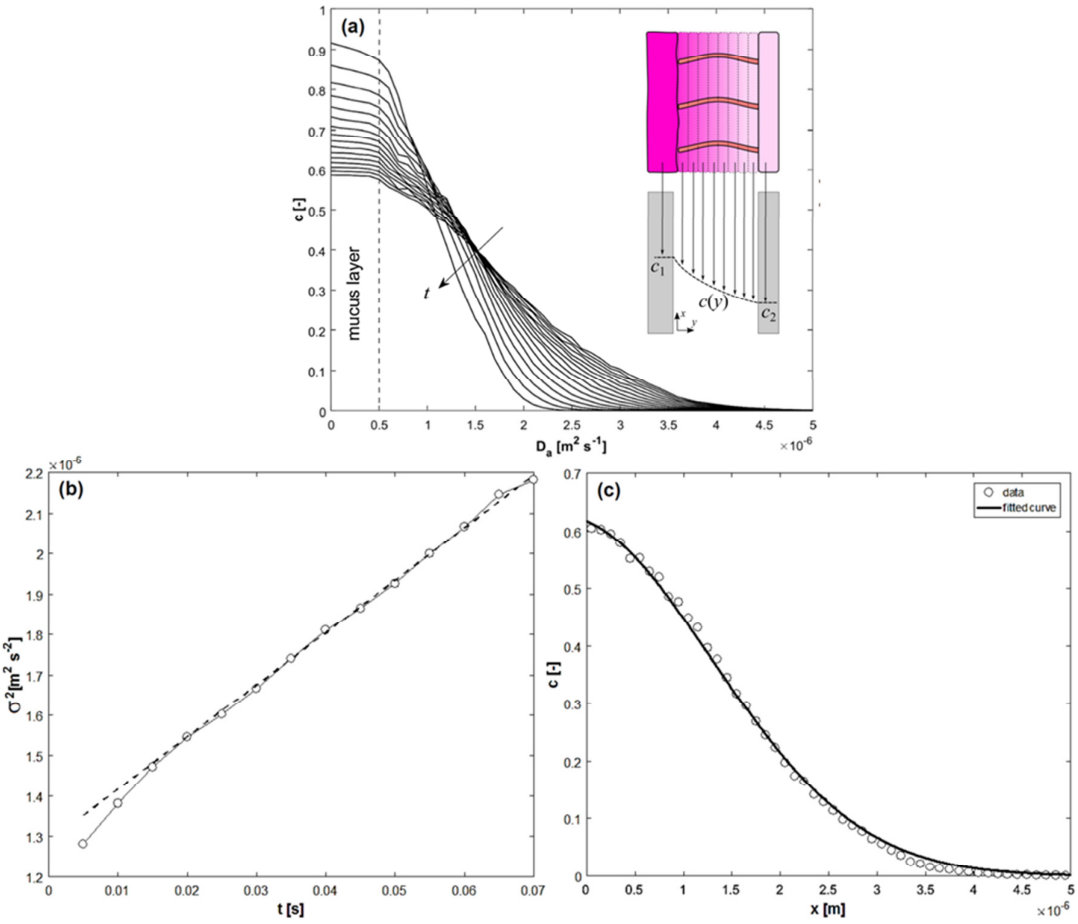

Fig. 7. Instantaneous concentration profiles in the y-direction (a), variance of the concentration versus time (b) and Gaussian fitting of the concentration profile at t = 0.08 s (c) for the case $D = 10^{-11}$ m^2 s^{-1}, f = 10 Hz, s = 2.5 μm.

Given Eq. (11), we can calculate the value of D_{pcl} from the concentration profiles of Fig. 7a. We compute the (time-dependent) variance σ^2 of each concentration profile, which, if the assumptions behind Eq. (11) are valid, should change linearly with time (Fig. 7b). The slope of Fig. 7b, therefore, gives the numerical value of D_{pcl}. The pseudo-diffusive hypothesis implies that the concentration profiles are approximately Gaussian, this is verified in Fig. 7c for the specific case of $D = 10^{-11}$ m^2 s^{-1}, f = 10 Hz, s = 2.5 μm. The same procedure for the

298 calculation of D_{pcl} is used for all the cases calculated in Table 1 and the results discussed in
299 the following sections.

300 *4.4 Shielding*

301 Fig. 8 shows how the Sherwood number changes with f and s in the case of $D = 10^{-11}$ m^2 s^{-1}.
302 $Sh < 1$ implies that the pseudo-diffusivity in the PCL is lower than the drug's molecular
303 diffusivity. This behaviour may look surprising at a first glance since convection can only
304 increase mixing and, therefore, it is not clear how the pseudo-diffusivity of the PCL can be
305 lower than the drug's molecular diffusivity.

306 The presence of the cilia, however, creates obstacles to the free motion of the drug in the fluid
307 and, therefore, reduces the apparent mass transfer in the PCL. We have named this
308 phenomenon shielding and indicate with D_{0pcl} the lowest apparent diffusivity, which occurs at
309 $f \rightarrow 0$ where no convective mixing is present. As f increases, the convective motion enhances
310 mass transfer and compensates the shielding effect as discussed in the next section

311

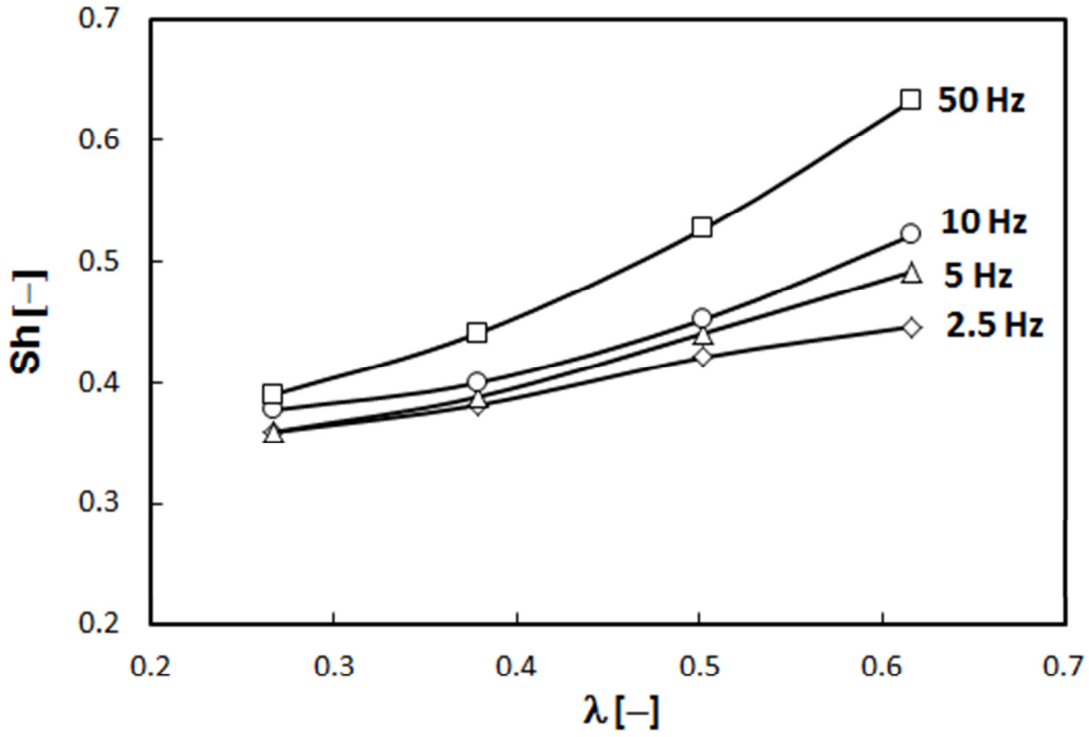

312

313 Fig. 8. Sherwood number for $D = 10^{-11}$ m^2 s^{-1} and various values of f and λ.

314 *4.5 Mass transfer regimes*

315 In Fig. 9 (*Sh* vs. *Pe*), we can distinguish three regions. Each of these regions is characterized
316 by different values of K and n in Eq. (9). We are interested, in particular, in the exponent n
317 and, therefore, we rewrite Eq. (9) as

$$D_{PCL} \propto s^{2n} f^{n} D^{1-n}. \tag{12}$$

318 Each value of n can be associate to a different mass transfer dynamics.

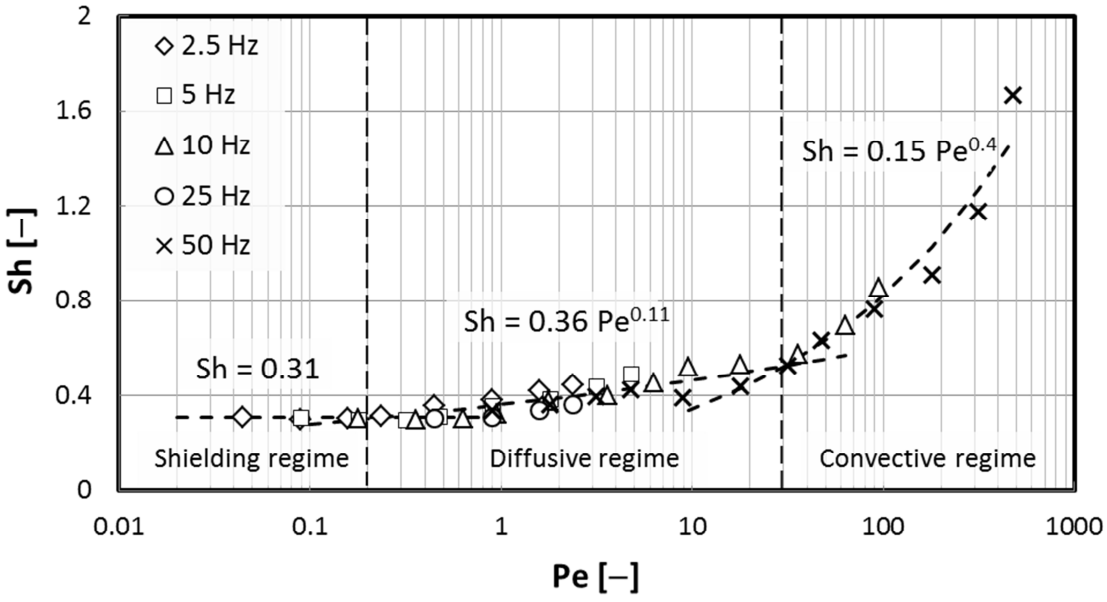

319

320 Fig. 9. Sherwood number versus Peclet number for all the simulations in Table 1.

321 Shielding regime ($Pe < 0.2$): the beat frequency is low and the shielding effect prevails. The
322 mass transfer only depends on the diffusivity since the frequency of the cilia beat is very slow,
323 but the pseudo-diffusivity is only one-third of the molecular diffusivity due to the shielding
324 effect. The value 0.31 would probably change in three-dimensional simulations, but the
325 general principle would remain valid. Considering Eq. (12) with $n = 0$,

$$D_{pcl} \propto D, \tag{13}$$

326 which confirms that the pseudo-diffusivity is proportional to the molecular diffusivity.

327 Diffusive regime ($0.2 < Pe < 30$): the cilia beat begins to 'open' the structure and allow higher
328 mass transfer in the ciliated-layer. Sh increases, but shielding is still high ($Sh < 1$).
329 Considering Eq. (12) with $n = 0.1$,

$$D_{pcl} \propto s^{0.2} f^{0.1} D^{0.9}, \tag{14}$$

which shows that diffusion is still the main mass transfer mechanics as, in Eq. (14), D has the highest exponent.

Convective regime ($Pe > 0.3$): the cilia beat creates significant recirculation regions that increase Sh. Considering Eq. (12) with $n = 0.4$,

$$D_{pcl} \propto s^{0.8} f^{0.4} D^{0.6}, \tag{15}$$

which indicates that the role of the frequency becomes more significant (its exponent is now 0.4). However, Eq. (15) also suggests that the size of the recirculation region (the exponent of s is 0.8) is even more important than the actual frequency.

5. Conclusions

In this paper, we have used the discrete multi-physics approach to simulate diffusive and convective mass transfer in boundary layers containing motile cilia. Fluids (mucus and PCL) and static solid (membrane) are implemented with the Smoothed Particle Hydrodynamics while flexible cilia are structured with the Mass-Spring model.

Metachronal wave is mimicked by means of "ghost parabola" particles and a mass transfer algorithm is introduced for modelling concentration diffusion between the mucus and the membrane through the PCL.

The aim of the present study is to quantify the effects of the ciliated layers on the PCL flow (convection) and mass transfer. Specifically, we have examined the role of the cilia beat frequency, the flexibility of the cilia and the initial diffusivity of the mucus.

The aim of the present study is to quantify the effects of the ciliated layers on the PCL flow (convection) and mass transfer. Specifically, we have examined the role of the cilia beat frequency, the flexibility of the cilia and the initial diffusivity of the mucus. The model accounts for several simplifications (2D geometry) and some of the complexities of the biological system are neglected. In particular, it does not account for microvilli above the ciliated cells, for discontinuities in the mucus layer and for presence of not-ciliated cells (e.g. goblet cells). We believe that these factors can potentially affect mass transfer in the ciliated layer to a certain degree. The physics behind the three mass transfer regimes (e.g. shielding, diffusive and convective), however, is expected to remain the same.

Mass transfer in the ciliated-layer is hindered by the presence of cilia and the apparent diffusivity reduces to one-third of the molecular diffusivity. As the frequency of the cilia beat

increases, recirculation regions appear in the velocity profile. In these regions, mass transfer increases due to convective mixing. However, the size of the convective regions seems to affect mass transfer more than the actual frequency. As a consequence of this, we suggest the possibility that the capacity of the respiratory epithelium to absorb inhaled drugs may be more strongly correlated with the flexibility of the cilia rather than the frequency of its beat. The current results could also have implications for our understanding of the mechanisms that lead to repeated infections and chronic respiratory syndrome in patients with ciliopathies. In patients with primary pulmonary ciliary dyskinesia or the more common form of acquired (secondary) ciliary dyskinesia the altered or completely suppressed function of the cilia reduces the effectiveness of the mucociliary "conveyor belt". As seen in this work, it also has important implications on the speed with which both drugs and toxic agents can reach the airway epithelium.

Acknowledgements

This article is based upon work from COST Action MP1404 SimInhale 'Simulation and pharmaceutical technologies for advanced patient-tailored inhaled medicines', supported by COST (European Cooperation in Science and Technology).

Supporting Information

A Appendix

B Appendix

C Appendix

D Appendix

REFERENCES

[1] Agnew JE, Sutton PP, Pavia D, Clarke SW. Radioaerosol assessment of mucociliary clearance - towards definition of a normal range. British Journal of Radiology. 1986;59:147-51.

[2] Smith DJ, Gaffney EA, Blake JR. Modelling mucociliary clearance. Respiratory Physiology & Neurobiology. 2008;163:178-88.

[3] Barton C, Raynor S. Analytical investigation of cilia induced mucous flow. Bulletin of Mathematical Biophysics. 1967;29:419-&.

[4] Blake JR. Mechanics of Muco-ciliary Transport. IMA Journal of Applied Mathematics. 1984;32:69-87.

[5] Mauroy B, Fausser C, Pelca D, Merckx J, Flaud P. Toward the modeling of mucus draining from the human lung: role of the geometry of the airway tree. Physical biology. 2011;8:056006.

[6] Lee WL, Jayathilake PG, Tan ZJ, Le DV, Lee HP, Khoo BC. Muco-ciliary transport: Effect of mucus viscosity, cilia beat frequency and cilia density. Computers & Fluids. 2011;49:214-21.

[7] Jayathilake PG, Tan Z, Le DV, Lee HP, Khoo BC. Three-dimensional numerical simulations of human pulmonary cilia in the periciliary liquid layer by the immersed boundary method. Computers & Fluids. 2012;67:130-7.

[8] Jayathilake PG, Le DV, Tan Z, Lee HP, Khoo BC. A numerical study of muco-ciliary transport under the condition of diseased cilia. Comput Methods Biomech Biomed Engin. 2015;18:944-51.

[9] Sedaghat MH, Shahmardan MM, Norouzi M, Jayathilake PG, Nazari M. Numerical simulation of muco-ciliary clearance: immersed boundary lattice Boltzmann method. Computers & Fluids. 2016;131:91-101.

[10] Chatelin R, Anne-Archard D, Murris-Espin M, Thiriet M, Poncet P. Numerical and experimental investigation of mucociliary clearance breakdown in cystic fibrosis. Journal of Biomechanics. 2017;53:56-63.

[11] Olsson B, Bondesson E, Borgstrom L, Edsbacker S, Eirefelt S, Ekelund K, et al. Pulmonary Drug Metabolism, Clearance, and Absorption. In: Smyth HDC, Hickey AJ, editors. Controlled Pulmonary Drug Delivery2011. p. 21-50.

[12] Alexiadis A. A smoothed particle hydrodynamics and coarse-grained molecular dynamics hybrid technique for modelling elastic particles and breakable capsules under various flow conditions. International Journal for Numerical Methods in Engineering. 2014;100:713-9.

[13] Alexiadis A. The Discrete Multi-Hybrid System for the Simulation of Solid-Liquid Flows. Plos One. 2015;10.

[14] Alexiadis A. A new framework for modelling the dynamics and the breakage of capsules, vesicles and cells in fluid flow. In: BarthesBiesel D, Blyth MG, Salsac AV, editors. Iutam Symposium on Dynamics of Capsules, Vesicles and Cells in Flow2015. p. 80-8.

[15] Alexiadis A, Stamatopoulos K, Wen W, Batchelor HK, Bakalis S, Barigou M, et al. Using discrete multi-physics for detailed exploration of hydrodynamics in an in vitro colon system. Computers in Biology and Medicine. 2017;81:188-98.

[16] Ariane M, Allouche MH, Bussone M, Giacosa F, Bernard F, Barigou M, et al. Discrete multi-physics: A mesh-free model of blood flow in flexible biological valve including solid aggregate formation. Plos One. 2017;12.

[17] Ariane M, Wen W, Vigolo D, Brill A, Nash FGB, Barigou M, et al. Modelling and simulation of flow and agglomeration in deep veins valves using discrete multi physics. Computers in Biology and Medicine. 2017:96-103.

[18] Leopold PL, O'Mahony MJ, Lian XJ, Tilley AE, Harvey BG, Crystal RG. Smoking Is Associated with Shortened Airway Cilia. Plos One. 2009;4.

[19] Boucher RC. Airway surface dehydration in cystic fibrosis: Pathogenesis and therapy. Annual Review of Medicine2007. p. 157-70.

[20] Wang Y, Gao Y, Wyss HM, Anderson PD, den Toonder JMJ. Artificial cilia fabricated using magnetic fiber drawing generate substantial fluid flow. Microfluidics and Nanofluidics. 2015;18:167-74.

[21] Aiello E, Sleigh M. Ciliary function of the frog oro-pharyngeal epithelium. Cell and Tissue Research. 1977;178:267-78.

[22] Sanderson MJ, Sleigh MA. Ciliary activity of cultured rabbit tracheal epithelium - beat pattern and metachrony. Journal of Cell Science. 1981;47:331-47.

[23] Marino MR, Aiello E. Cinemicrographic analysis of beat dynamics of human respiratory cilia. J Progress in clinical and biological research. 1982;80:35-9.

[24] Gheber L, Priel Z. Extraction of cilium beat parameters by the combined application of photoelectric measurements and computer simulation. Biophysical Journal. 1997;72:449-62.

[25] Chilvers MA, O'Callaghan C. Analysis of ciliary beat pattern and beat frequency using digital high speed imaging: comparison with the photomultiplier and photodiode methods. Thorax. 2000;55:314-7.

[26] Chilvers MA, Rutman A, O'Callaghan C. Functional analysis of cilia and ciliated epithelial ultrastructure in healthy children and young adults. Thorax. 2003;58:333-8.

[27] Chilvers MA, Rutman A, O'Callaghan C. Ciliary beat pattern is associated with specific ultrastructural defects in primary ciliary dyskinesia. Journal of Allergy and Clinical Immunology. 2003;112:518-24.

[28] Fahrni F, Prins MWJ, van Ijzendoorn LJ. Micro-fluidic actuation using magnetic artificial cilia. Lab on a Chip. 2009;9:3413-21.

[29] Eixarch H, Haltner-Ukomadu E, Beisswenger C, Bock U. Drug Delivery to the Lung: Permeability and Physicochemical Characteristics of Drugs as the Basis for a Pulmonary Biopharmaceutical Classification System (pBCS). Journal of Epithelial Biology & Pharmacology. 2010;3:1-14.

453 [30] Oldenburg AL, Chhetri RK, Hill DB, Button B. Monitoring airway mucus flow and ciliary activity
454 with optical coherence tomography. Biomedical Optics Express. 2012;3:1978-92.

455 [31] Bird R, B., Stewart W, E., Lightfoot E, N. Transport phenomena. John Wiley & Sons, Revised 2nd
456 Edition edition ed2007.

457

458

Appendix A

The DMP version used in this study links SPH and MSM. In this section, we provide a brief introduction to these techniques and how they are coupled together.

1. Smoothed Particle Hydrodynamics (SPH)

The SPH equations of motion are obtained from the discrete approximations of the Navier-Stokes equation at a set of points, which can be thought as particles characterized by their own mass, velocity, pressure and density. The fundamental idea behind this approximation lies in the identity

$$f(\mathbf{r}) = \iiint f(\mathbf{r}')\delta(\mathbf{r}\text{-}\mathbf{r}')d\mathbf{r}', \qquad \text{(A.1)}$$

where $f(\mathbf{r})$ is a generic function defined over the volume V, the vector $\mathbf{r}$ is a three-dimensional point in V and $\delta(\mathbf{r})$ is the three-dimensional delta function. In the SPH formalism, the delta function is approximated by a smoothing Lucy kernel W with characteristic width h (smoothing length) such that

$$\lim_{h\to 0} W(\mathbf{r},h) = \delta(\mathbf{r}) . \qquad \text{(A.2)}$$

This brings to the approximation

$$f(\mathbf{r}) \approx \iiint f(\mathbf{r}')W(\mathbf{r}\text{-}\mathbf{r}',h)d\mathbf{r}', \qquad \text{(A.3)}$$

which can be discretised over a series of particles of mass $m = \rho(\mathbf{r})d\mathbf{r}$ obtaining

$$f(\mathbf{r}) \approx \sum_i \frac{m_i}{\rho_i} f(\mathbf{r}_i)W(\mathbf{r}\text{-}\mathbf{r}_i,h), \qquad \text{(A.4)}$$

where m_i and ρ_i are the mass and density of the i^{th} particle, and i ranges over all particles within the smoothing kernel (i.e. $|\mathbf{r}-\mathbf{r}_i| < h$). Equation (A.4) represents the discrete

479 approximation of a generic continuous field and can be used to approximate the Navier-Stokes
480 equation

481 $$m_i \frac{dv_i}{dt} = \sum_j m_i m_j \left(\frac{P_i}{\rho_i^2} + \frac{P_j}{\rho_j^2} + \Pi_{i,j}\right)\nabla_i W_{i,j} + \mathbf{f}_i, \qquad \text{(A.5)}$$

482 where v_i is the velocity of particle i, $W_{i,j}$ means $W(\mathbf{r_j}\text{-}\mathbf{r_i}, h)$, ∇_i denotes the gradient of the
483 kernel with respect of the coordinate r_i, P is the pressure, $\mathbf{f}_i$ a volumetric body force, and $\Pi_{i,j}$
484 introduces the viscous forces. Various expressions for the tensor $\Pi_{i,j}$ are available; here we
485 use (Monaghan and Gingold 1983)

486 $$\Pi_{i,j} = -\alpha h \frac{c}{\rho_{ij}} \frac{v_{ij} \mathrm{r}_{ij}}{\mathrm{r}_{ij}^2 + bh^2}, \qquad \text{(A.6)}$$

487 where α is a parameter (~ 1) used to ensure the stability of the simulation, c is the artificial
488 sound speed in the liquid and b is a constant introduced to avoid singularities in the case of
489 very close particles ($b \approx 0.01$). The value of α depends on the specific type of simulation; in
490 this study we use $\alpha = 1$ as done in previous studies (Ariane et al. 2017a).

491 In order to close Eq. A.5, an equation of state linking ρ and P is required. In this paper, we
492 use Tait's equation

493 $$P(\rho) = \frac{c_0 \rho_0}{7}\left[\left(\frac{\rho}{\rho_0}\right)^7 - 1\right], \qquad \text{(A.7)}$$

494 where c_0 and ρ_0 are, respectively the sound speed and density at zero applied stress.

495

496

2. Mass-Spring modelling (MSM) / Coarse-Grained Molecular Dynamics (CGMD)

Molecular dynamics is a form of investigation where the motion and the interaction of a certain number of computational atoms or molecules are studied. In classical MD simulations atoms move according to the Newtonian equations of motion

$$m_i \frac{dv_i}{dt} = -\frac{\partial}{\partial \mathbf{r}} U_{tot}(\mathbf{r}_1, \mathbf{r}_2, ...\mathbf{r}_N), \quad \text{(A.8)}$$

where U_{tot} is the total interatomic potential, which can be divided into two main parts: non bonded and intramolecular. Non bonded forces are usually represented by the so-called Lennard-Jones potential, while the intramolecular forces are often divided in subgroups e.g.

$$U_{intramolecular} = U_{bond} + U_{angle} \quad \text{(A.9)}$$

Each of these potentials can have different forms. In this study, we use the harmonic bond potential

$$U_{bond} = k_b (r - r_0)^2, \quad \text{(A.10)}$$

where k_b a Hookean coefficient, r_0 the equilibrium distance, and the harmonic angle potential

$$U_{angle} = k_a (\theta - \theta_0)^2, \quad \text{(A.11)}$$

where k_a is an angular Hookean coefficient and θ_0 the equilibrium angle,

Equations (A.9─A.11) are the basis for the ball-and-stick representation of molecules that can be coarse-grained to model macroscopic solids within the MSM framework. This approach can be employed to model macroscopic phenomena such as stretching and bending of solids under the effect of external forces. In the case under investigation, we divide the membrane in a certain number of notional particles and use the potentials of Eq. A.10 and A.11 to simulate its deformation. Figure 1 shows how bond and angle potentials are used in the membrane

model. This component of the DMP has been indicated sometimes as MSM and sometimes as CGMD. The mathematical formulation is the same: at small scales (e.g. microfluidic applications) the term CGMD is preferred (Alexiadis 2014), at larger scales the term MSM is preferred (Alexiadis et al. 2017).

3. Coupling the two models

The interaction between the solid (MSM particles) and the liquid (SPH particles) is defined by boundary conditions, which relate the behaviour of two adjacent materials at the common interface. There are three main types of phenomena that must be taken into consideration in designing these boundary conditions (Müller et al. 2004): no-penetration, no-slip and continuity of stresses. In continuum mechanics, these conditions are often represented as

$$(\frac{\partial}{\partial t}\mathbf{u} - \mathbf{v}) \cdot \mathbf{n} = \mathbf{0} \ \text{(no – penetration)}, \tag{A.12}$$

$$(\frac{\partial}{\partial t}\mathbf{u} - \mathbf{v}) \times \mathbf{n} = \mathbf{0} \ \text{(no – slip)} \tag{A.13}$$

and

$$\sigma_s \mathbf{n} = \sigma_f (-\mathbf{n}) \ \text{(continuity of stresses)} \tag{A.14}$$

where **n** is the normal to the boundary, **u** the displacement of the solid, **v** the velocity of the liquid, σ_s the stresses in the solid and σ_f in the fluid.

In the particle framework, various no-penetration methods can be implemented (Ferrand et al. 2013) and an additional central force of the Lennard-Jones type is often used

$$f(r) = K\left[\left(\frac{r^*}{r}\right)^{n_1} - \left(\frac{r^*}{r}\right)^{n_2}\right]\frac{\mathrm{r}}{r^2}, \tag{A.15}$$

where r^* represents the repulsive radius of the particle, and n_1 and n_2 are usually set to 4 and 2, although also the original 12-6 Lennard-Jones values are sometimes used. The constant K is chosen on the basis of a characteristic velocity of the flow.

Concerning the "ghost parabola", we use a softer repulsion potential based on a cosines form that only push apart overlapping cilia particles

$$f(r) = K_s\left[1 + cos\left(\frac{\pi.r}{r^*}\right)\right], \qquad \text{(A.16)}$$

With K_s a constant chosen arbitrarily according to the simulations.

The no-slip condition models the friction between the solid and the fluid. In finite-element numerical methods it is enforced by imposing that the two materials have the same velocity at the interface. The advantage of using a particle-particle representation is that, once both the no-penetration and no-slip boundary condition are enforced, the continuity of stress is automatically satisfied by the equation of motion (A.5).

References

Ferrand, M., D. R. Laurence, B. D. Rogers, D. Violeau and C. Kassiotis (2013). "Unified semi-analytical wall boundary conditions for inviscid, laminar or turbulent flows in the meshless SPH method." International Journal for Numerical Methods in Fluids 71(4): 446-472.

Monaghan, J. J. and R. A. Gingold (1983). "Shock simulation by the particle method SPH." Journal of Computational Physics 52(2): 374-389.

Müller, M., S. Schirm, M. Teschner, B. Heidelberger and G. M (2004). "Interaction of fluids with deformable solids." Computer Animation and Virtual Worlds W 15: 159-171.

559 **Appendix B**

560 There are two types of parameter required for the simulations: model parameters and
561 simulation parameters. Table B.1 list the numerical values used in the model parameters
562 (simulation parameters are discussed in section 2 of the manuscript).

563 **Table B.1. Model parameters used in the simulations.**

SPH (eqs. A.5−A.7)	
Parameter	**Value**
Number of membrane particles (10 layers)	3270
Number of PCL particles	19788
Number of mucus particles N_{mucus}	7050
Number of cilium particles (36 cilia)	2592 (72 particles/cilium)
Number of Ghost parabola particles (1 layer)	343
Mass of each particle	$4.3.\cdot10^{-12}$ kg
Initial distance among particles Δr	$6.6\cdot10^{-8}$ m
Smoothing length h	$1.98\cdot10^{-7}$ m
Artificial sound speed c_0	0.25 m s^{-1}
Density of PCL ρ	1000 kg m^{-3}
Density of mucus ρ	1000 kg m^{-3}
Dynamic viscosity of PCL μ	1 10^{-3} Pa s
Dynamic viscosity of mucus μ	20 Pa s
Time step Δt	10^{-8} s
MSM (eqs. A.8-A.11)	
Parameter	**Value**
Angular coefficient k_a	1.0 10^{-12} J
Hookian coefficient k_b	20 J m^{-2}
Equilibrium distance r_0	$6.6\cdot10^{-8}$ m
BOUNDARIES (Eq. A12-A.15)	
Constant K	5 10^{-16} J
Constant Ks	8 10^{-15} J
Repulsive radius r*	1.65 10^{-7} m

564 The viscoelastic properties of the mucus are discussed in Appendix C.

565
566

Appendix C

To model viscoelastic fluids in discrete multi-physics, we can implement the viscosity via SPH forces (see Appendix A) and add the elasticity as an equivalent attractive force

$$k_b = \frac{EA_0}{L_{mu}}, \tag{C.1}$$

where k_b is the Hookean bending coefficient of Eq. A.10, E the Young modulus of mucus, A_0 the sectional area and L_{mu} the thickness of the mucus layer.

Moreover, since the elastic force is shared by all the mucus particles $k^*=k_b/N_{mucus}$, where N_{mucus} is the number of computational particles used for the mucus layer. Mucus is a viscoelastic fluid and not a viscoelastic solid, consequently, we cannot use actual Hookean springs that would prevent relative motion of the fluid particles. Therefore, we approximate locally the harmonic potential with a Lennard Jones form with the minimum in the same position. This implies that the second derivative of both potentials should be the same at r_0 e.g.

$$\frac{dU_{IJ}}{dr^2} = \varepsilon\left[156\frac{r_0^{12}}{r^{14}} - 84\frac{r_0^6}{r^8}\right] = 72\varepsilon \text{ at } r = r_0, \tag{C.2}$$

which gives $\varepsilon = k^*/72$.

In our case, E = 10 Pa ; N_{mucus} = 7050, L_{me} = $0.6\cdot10^{-6}$ m and, therefore, $\varepsilon = 1\cdot10^{-6}$ J. This produces a Maxwell viscoelastic material with μ = 20 Pa s and E = 10 Pa.